OUKA
The University of Osaka
Institutional Knowledge Archive

Title	Time-resolved spectroscopic mapping of vibrational energy flow in proteins: Understanding thermal diffusion at the nanoscale
Author(s)	Mizutani, Yasuhisa; Mizuno, Misao
Citation	Journal of Chemical Physics. 2022, 157(24), p. 240901
Version Type	AM
URL	https://hdl.handle.net/11094/91291
rights	This article may be downloaded for personal use only. Any other use requires prior permission of the author and AIP Publishing. This article appeared in The Journal of Chemical Physics 157, 240901 (2022) and may be found at https://doi.org/10.1063/5.0116734.
Note	

The University of Osaka Institutional Knowledge Archive : OUKA

https://ir.library.osaka-u.ac.jp/

The University of Osaka

Time-resolved Spectroscopic Mapping of Vibrational Energy Flow in Proteins: Understanding Thermal Diffusion at the Nanoscale

Yasuhisa Mizutani[†*] *and Misao Mizuno*[†*]

[†] Department of Chemistry, Graduate School of Science, Osaka University, 1-1 Machikaneyama, Toyonaka, Osaka 560-0043, Japan

[*]Corresponding author

Corresponding Author

Yasuhisa Mizutani — *Department of Chemistry, Graduate School of Science, Osaka University, 1-1 Machikaneyama, Toyonaka, Osaka 560-0043, Japan*; orcid.org/ 0000-0002-3754-5720; Email: mztn@chem.sci.osaka-u.ac.jp

Misao Mizuno — *Department of Chemistry, Graduate School of Science, Osaka University, 1-1 Machikaneyama, Toyonaka, Osaka 560-0043, Japan*; orcid.org/0000-0003-2206-1763; Email: misao@chem.sci.osaka-u.ac.jp

ABSTRACT

Vibrational energy exchange between various degrees of freedom is critical to barrier-crossing processes in proteins. Hemeproteins are well suited for studying vibrational energy exchange in proteins because the heme group is an efficient photothermal converter. The released energy by heme following photoexcitation shows migration in a protein moiety on picosecond timescale, which is observed using time-resolved ultraviolet resonance Raman spectroscopy. The anti-Stokes ultraviolet resonance Raman intensity of a tryptophan residue is an excellent probe for the vibrational energy in proteins, allowing mapping of energy flow with the spatial resolution of a single amino acid residue. This Perspective provides an overview of studies on vibrational energy flow in proteins, including future perspectives for both methodologies and applications.

I. INTRODUCTION

The rates of a chemical reaction depend on how often a nuclear motion that transforms reactants into products acquires energy sufficient to cross the activation barrier. In solutions and other condensed phases, the required energy is provided to the reactive mode through intramolecular and intermolecular energy transfer. The relative rate of supplying energy to the reactive mode compared to those for energy transfer to the solvent and unreactive solute modes may determine the rates, pathways, and efficiency of the reaction. Vibrational dynamics are therefore ultimately responsible for the evolution of a molecule.

Intermolecular energy transfer in materials is regarded macroscopically as thermal diffusion, which can be described by the Fourier's law of heat conduction. However, it is not obvious that the familiar concepts of thermal diffusion through continuum media apply to energy transfer at the nanoscale because thermal energy at this scale is transported through a molecule by discrete molecular vibrations. Since energy transport is central to the operation of molecular machinery, at the level of individual molecules, it is necessary to examine the microscopic description of intermolecular energy transfer.

Intramolecular and intermolecular vibrational energy transfer in solutions has been widely studied using time-resolved vibrational spectroscopy.[1-9] Excess vibrational energy is deposited into the solute molecules by an ultrashort laser pulse. Subsequent vibrational energy redistribution is investigated by monitoring both population decay of the initially excited modes and the buildup of populations in accepting modes in the solute and solvent molecules. Much experimental work has focused on understanding intramolecular and intermolecular vibrational energy transfer in solutions. Intramolecular vibrational transfers in solute molecules in solutions occurs in the subpicosecond to picosecond time region,[1-9] with energy relaxations via two

consecutive steps being commonly observed.[10-26] In the first step, energy is transferred from the initially excited vibrational mode to several selected other vibrational modes of the molecule. In the second step, the energy is transferred to all other modes of the molecule, resulting in the excess energy being equilibrated over all degrees of freedom. Intermolecular vibrational energy transfers take place at the 1-100 ps timescale in solutions.[27-29] The excess energy flows out of the solute molecule into the solvent degrees of freedom as the solute molecule relaxes to its locally thermalized state. However, although studies in solutions provide insights into intermolecular vibrational energy transfer, it is difficult to study the distance dependence of vibrational energy transfer because the configurations of molecules in solutions randomly change with time. Time-resolved spectroscopic measurements of organized systems such as micelles[30] and molecular monolayers[31-33] have attempted to obtain a detailed picture of intermolecular energy transfer. The observed linear dependence on the length of an alkyl chain of the time required for vibrational transfer across the chains indicates that the leading edge of the excess vibrational energy propagates ballistically along the alkyl chains in the monolayers. Vibrational energy transport between energy-releasing and probing groups connected by an aliphatic chain was studied with time-resolved infrared spectroscopy.[34-42] However, very little is known regarding energy transfer over longer distances.

The well-defined structures of proteins provide us ideal opportunities to study intermolecular vibrational energy transfer since proteins spontaneously fold into unique three-dimensional structures. Moreover, vibrational energy transfer is essential to understanding reactions in proteins.[43] Such reactions occur in specific active sites, with the surrounding protein moiety serving as a medium for the active sites. Therefore, how a protein moiety dissipates the excess

energy generated by the reaction or transports the energy to activate the active site is key to understanding reactions in proteins.

In this Perspective, we summarize the research on vibrational energy transfer in proteins conducted over the last decade. Our research described in this Perspective was prompted by the simple question "What does thermal diffusion look like microscopically?" As mentioned above, it is not obvious that much of our understanding of macroscopic energy dissipation is applicable to microscopically describing energy dissipation. Furthermore, energy distribution in a only locally relaxed state may differ from a statistical distribution. Thus, because of our limited understanding of microscopic energy transfer in condensed phases, we studied vibrational energy transfer using the stable and well-defined structures of proteins. Schematics of macroscopic and microscopic views of thermal diffusion are shown in Figure 1. To study vibrational energy transfer in proteins, we first had to develop appropriate experimental techniques and apparatuses. Our experimental techniques, as well as the techniques of other research groups, are described in Section II. We have then examined in detail vibrational energy flow in proteins from various aspects. Our studies on the distance dependence of energy flow in proteins and the mechanism of energy transduction are described in Sections III and IV, respectively. Microscopic view of vibrational energy flow in proteins is discussed in Section V. Section VI describes the quantitative characterization of the amount of excess energy in a single amino acid residue in proteins. In general, if energy possessed by each molecule does not follow a statistical distribution, the temperature cannot be defined. Still, using the assumption that all the accessible microstates of the molecule are equally probable, if the molecule has many vibrational degrees of freedom and if the excess energy is large, the occupation probabilities in the vibrationally excited states of the molecule in nonequilibrium are close to a Boltzmann distribution at higher

temperature. We discuss vibrational density of states and occupation probability in the vibrationally excited states in Section VI. The high efficiency of energy flow in proteins is utilized for microscopic heating on the molecular scale, making proteins excellent molecular heaters. The development of protein heaters is described in Section VII. We discuss the outlook for studies on vibrational energy transfer in proteins in Section VIII. Finally, we summarize the discussions provided in this Perspective in Section IX.

II. EXPERIMENTAL TECHNIQUES AND PAST STUDIES

Observation of intermolecular vibrational energy transfer requires an energy source group (*heater* group) and an energy probe group (*probe* group), together with a well-defined distance and relative orientation of the two groups. Stable structures of proteins keep the distance and relative orientation between a pair of heater and probe groups constant.

A. Pump techniques

Excess vibrational energy can be deposited into proteins through direct excitation of vibrational modes and through indirect excitation via nonradiative transitions following electronic excitations. A specific vibrational mode can be excited by an infrared pulse. For example, the stretching mode of carbonyl groups shows strong infrared absorption, and its energy is relatively high (1620–1750 cm^{-1}).[44] The C–D stretching modes of deuterated Leu residues were excited by an infrared pulse of 2200 cm^{-1}.[45] Ultrafast nonradiative transition is an excellent photothermal conversion technique since the electronic energy obtained by the electronic transitions with a visible pulse is distributed into the vibrational degrees of freedom. For example, metalloporphyrin and malachite green have been utilized as heater dyes because they bind to specific sites in bovine serum albumin.[46] Heme is a natural cofactor in hemeproteins

and serves as an efficient molecular heater. Azobenzene[44, 47-49] and azulene[50-54] covalently linked to a polypeptide chain were shown to be excellent photothermal converters upon visible excitation. We will discuss the exceptional properties of heme in this context in detail later. Unnatural amino acids whose side chain contains a moiety conducive to ultrafast nonradiative transition are excellent molecular heaters.[50-54] Pump techniques used to date are summarized in Table I.

B. Probe techniques

Populations of vibrationally excited states can be monitored by hot bands in infrared absorption spectra and by anti-Stokes bands in Raman spectra. Absorption bands of vibrationally excited states are located at lower frequency than those of the vibrational ground state due to vibrational anharmonicity. The C=O stretching band of an isotopically labeled carbonyl group in the main chain of an amino acid has been used as a site-selective probe.[44, 45, 47, 48, 55] Infrared absorption bands of side chains of both natural and unnatural amino acids can be excellent probes.[50-54] Anti-Stokes scattering originates from vibrationally excited states and is thus suitable for monitoring populations of vibrationally excited states. Changes in vibrationally excited populations can be discriminated from structural changes by comparison of temporal changes between Stokes and anti-Stokes intensities, which is an advantage of Raman spectroscopy over infrared spectroscopy. In addition, since the resonance effect using ultraviolet light selectively enhances the Raman bands of aromatic amino acid residues,[56-60] ultraviolet resonance Raman (UVRR) spectroscopy enables site-selective detection of excess energy at the level of a single residue in a large protein molecule. Probe techniques used to date are summarized in Table II.

C. Studies on peptides

Peptides are advantageous for studying vibrational energy transfer in short distances because their structures are less complex than those of proteins. Pioneering studies on vibrational energy transfer along short peptide polypeptide chains were carried out by Hamm and coworkers.[44, 45, 47, 48, 55] They systematically isotope-labeled the carbonyl groups of the main chain of helical peptides as site-selective probes of vibrational energy transfer by time-resolved infrared spectroscopy. Vibrational energy was locally deposited at the N-terminus of the helices by ultrafast energy conversion of azobenzene[44, 47, 48] and gold nanoparticles[55] excited by visible pulses. Placing the isotope label at different positions in the helix allowed measurement of the local temperature at various distances from the heat source as a function of time. Another method of vibrational excitation is infrared excitation of the C=O stretching mode of the polypeptide chain[44] and the C–D stretching modes of a deuterated Lue residue.[45] These studies showed that vibrational energy propagation can be described as a diffusion-like process at room temperature. The temperature dependence of vibrational energy transfer suggested that structural flexibility enhances vibrational energy transfer by redistributing the excess energy into a few vibrational modes that delocalize over large parts of the molecule.[48]

β-hairpin fold peptides containing a pair of nonnatural amino acids as heater and probe residues were used to elucidate the mechanism of vibrational energy transfer.[53] The temporal changes of the vibrationally excited populations in the probe residues of four variants with the heater-probe pair at different positions were systematically studied. Three of the variants had the heater-probe pair on opposing strands at different backbone distances, while one had the pair on the same strand. The experimental data, combined with computational results, showed that energy transfer between opposite β-strands is dominated by contact pathways.

D. Hemeproteins

Numerous studies of vibrational energy transfer have been carried out using hemeproteins. Hemeproteins are ideal molecular systems to study energy transfer because a photoexcited heme group is converted to the electronic ground state via ultrafast internal conversion within 100 fs.[61, 62] Excess vibrational energy as high as 25000 cm^{-1} can thus be deposited locally at the heme site in proteins immediately after photoexcitation via the Soret transition. Consequently, heme acts as a very efficient photothermal energy convertor. Indeed, we previously showed that the excess energy is released within 1-2 ps from the heme site,[63-65] demonstrating that heme acts as an efficient heater molecule. The excess energy transferred from the heme group subsequently flows into the protein moiety, then finally the energy is dissipated into solvent water over a few tens of picoseconds.[66-68] Thus, the time scales of energy relaxation of the heme group and energy dissipation from the protein moiety to water are well characterized. By contrast, there have been no direct observations and little is known about energy flow in protein moieties.

To address this issue, we used time-resolved UVRR spectroscopy. Anti-Stokes UVRR spectroscopy on amino acid residues can provide information on the excess energy in the observed residues. Although our idea of observing vibrational energy flow in proteins appeared promising, no measurements had previously been reported for probing energy flow in a protein moiety based on the anti-Stokes UVRR intensities of Trp residues in the protein. We directly observed vibrational energy flow in ferric cytochrome *c* in a "proof-of-principle" experiment, demonstrating the excellence of time-resolved anti-Stokes UVRR Raman spectroscopy for examining vibrational energy flow in proteins.[69] Cytochrome *c* was selected because, as can be seen in Figure 2A, it has a single intrinsic tryptophan residue (Trp59 in bovine cytochrome *c*) close to the heme group. Temporal evolutions of anti-Stokes UVRR intensities of the Trp59

residue reflected the kinetics of energy flow transferred from heme and energy release of the Trp residue in cytochrome *c*.

Figure 2B shows the anti-Stokes UVRR spectra of ferric cytochrome *c* pumped with 405 nm pulse and probed with 230 nm pulse. An anti-Stokes UVRR spectrum recorded only with the probe pulse is shown in the top trace. The spectrum contains the UVRR bands for Trp at 759 (W18 mode), 876 (W17 mode), and 1015 cm^{-1} (W16 mode), and a band for Tyr at 1181 cm^{-1} (Y9a mode). The mode assignments made by Harada and coworkers were adopted.[56] The W16, W17, and W18 modes are out-of-phase indole ring breathing, benzene ring deformation and in-plane NH bending, and in-phase indole ring breathing modes of the Trp side chain, respectively. The Y9a mode is an in-plane CH bending mode of the Tyr side chain. The band at 1599 cm^{-1} was not attributed to any vibrational mode of aromatic amino acid residues. The asterisk-marked band at 983 cm^{-1} was derived from sulfate ion introduced as an internal reference for calculating Raman intensities. The anti-Stokes bands in the probe-without-pump spectrum arise from thermal populations of the vibrationally excited states at room temperature. The 405-nm pump pulse electronically excites heme. At each delay time, the probe-without-pump spectrum was subtracted from the probe-with-pump spectrum to yield the pump-induced difference spectrum. Positive anti-Stokes bands in the difference spectra reflect the vibrationally excited populations of the residues due to the excess energy released by heme. Positive anti-Stokes Raman bands of the Trp and Tyr residues were observed in the difference spectrum at 5 ps and vanished within 30 ps in the anti-Stokes UVRR difference spectra. Figures 2C and 2D show the temporal evolutions of the area intensities of the W18 and W16 bands, respectively, in the time-resolved difference spectra relative to those in the probe-without-pump spectrum. Intensity changes of the W16 and W18 bands were fitted to a double-exponential function expressing the rise and the

decay, convoluted with the instrument response function. Time constants of the rise and decay of the anti-Stokes W16 band were determined to be 5.6_7±3.0 and 5.6_8±3.0 ps, respectively. For the anti-Stokes W18 band, the rise and decay time constants were calculated to be 5.5±2.5 and 5.6±2.5 ps, respectively. We found that Stokes W16 and W18 bands also changed intensity upon photoexcitation, presumably due to a photoinduced change in a hydrogen bond between the Trp59 and heme, indicating that the Raman cross-sections had temporally changed. Taking the intensity ratio of the anti-Stokes to the Stokes bands allowed estimation of the inflow and outflow rates of vibrational energy for Trp59 as 1–3 and ~8 ps, respectively. These results showed that time-resolved UVRR spectroscopy is excellent for investigating the flow of vibrational energy in proteins.

Energy dissipation from a protein to the solvent water has been studied using femtosecond time-resolved infrared[68] and transient phase grating techniques[66, 67] that monitor heating of the solvent water caused by heme photoexcitation. These studies showed that the excess energy was transferred to the solvent water through the protein matrix in a few tens of picoseconds. The time constant of energy release from Trp59 in cytochrome *c* was less than the time constant of water heating, indicating that energy released from Trp59 is transmitted to the solvent water through the remaining protein matrix. It is unlikely that Trp59 transfers energy directly to the solvent water since it has no exposed contact sites.[70]

III. DISTANCE DEPENDENCE OF ENERGY FLOW

A. Myoglobin: globular protein

The “proof-of-principle” experiments using cytochrome *c* described in the preceding section clearly demonstrated that time-resolved anti-Stokes UVRR spectroscopy on aromatic amino acid

residues is a powerful tool for studying vibrational energy flow in a protein. Combining this method with site-directed mutagenesis led to even greater advancements because amino acid substitution can alter the location of a Trp residue inside a protein. [71] It is possible to map energy flow in a protein by systematically changing the position of the Trp residue with respect to the heme group and comparing the temporal evolutions of the Trp residues in the mutants. Thus, hemeproteins offer significant advantages for analyzing energy transport in the condensed phase because the distance and relative orientation of the heater (heme) and probe groups (Trp residue) can be manipulated in proteins.

We carried out systematic measurements on myoglobin, a representative hemeprotein, using the aforementioned advantages of hemeproteins. In addition, myoglobin is attractive for physicochemical studies because it is stable, well expressed in *Escherichia coli*, and extensively characterized in terms of its structure and dynamics.[72-77] Mutants involving a single Trp residue at different positions are required for systematic mapping of the excess energy. Two Trp residues, Trp7 and Trp14, are present in wild-type (WT) sperm whale myoglobin. First, a plasmid lacking Trp residues was constructed by nucleotide replacements for Trp7 and Trp14 with Tyr and Phe, respectively.[78] Then, we created plasmids for three mutants with a single Trp at a particular location. Figure 3A shows the myoglobin mutants prepared. One mutant contains a Trp residue at position 68, of which center-to-center distance to heme is 6.8 Å (PDB ID code 2OH9). Another mutant possesses a Trp residue at position 28, with a 12.4 Å distance to heme (PDB ID code 2OH8). Trp7 was replaced with Tyr in the third mutant, whereas Trp14 remained unchanged; the distance between heme and Trp14 is 15.0 Å. Each of the three mutants had a Trp residue in a similar direction from the heme group, but at significantly different distances. The three-dimensional structures of these mutants are very similar to that of WT myoglobin, as

evidenced by crystallographic data.[79] Thus, analysis of the distance dependence of energy transfer from heme to the Trp residue was made possible by comparison of the results utilizing these three mutants.

Figures 3B and 3C depict the temporal evolution of the W16 and W18 anti-Stokes intensity in the time-resolved difference spectra relative to that in the probe-without-pump spectrum. The anti-Stokes intensities of the mutants reflect the amount of energy delivered to the Trp residue at different positions in the protein. The data in Figure 3B show that the amplitude of the anti-Stokes intensities decreased as the heme–Trp distance increased. This behavior can be qualitatively explained by the classical thermal diffusion model, showing that excess energy becomes spatially less dense as the energy diffuses in the protein. It is interesting to compare the time constants of the rise at the different positions. For the W16 band, the Trp68 and Trp28 mutants exhibited rise time constants of 3.0±0.7 and 4.9±1.1 ps, respectively. For the W18 band, the rise time constants for Trp68 and Trp28 mutants were determined to be 3.0±0.4 and 4.0±0.6 ps, respectively. Trp28 consistently had a longer rise time than Trp68, showing that it takes longer for excess energy to reach at position 28 (12.4 Å) than at position 68 (6.8 Å). Consequently, the observed distance dependence is qualitatively compatible with classical thermal diffusion. In this work, energy dissipation in a protein moiety at multiple positions was directly observed with a spatial resolution of an amino acid residue for the first time.

Next, these observed data were quantitatively compared with data calculated based on a classical two-boundary thermal diffusion model by Li and Champion[80] to simulate the thermal dynamics of transient cooling in hemeproteins following excitation of heme. Using the model, we determined the temperature distribution throughout the protein. The computed temperature is shown in Figure 3D as a function of time and the heme–Trp distance. The Boltzmann factor was

used to explain how the anti-Stokes Raman intensity varied with temperature. The computed temperature was converted to the Boltzmann factor for the W18 and W16 modes to estimate the temporal changes of the anti-Stokes Raman intensities, which are represented by the broken lines in Figures 3B and 3C. The model properly reproduced the temporal evolution of the anti-Stokes intensities of the W16 and W18 bands for the Trp68 and Trp28 mutants, but not for the Trp14 mutant. Thus, the classical thermal transport model is unable to quantitatively reproduce the entire data set, suggesting that protein matrices are not uniform thermal conductors. These experimental data validate a conclusion from theoretical work showing that energy flow is intrinsically anisotropic due to the geometry of proteins.[81]

B. Cytochrome b_{562}: four-helix bundle protein

Although myoglobin has advantages for studies on vibrational energy flow, the structure of its main chain is complex. This makes altering the location of the probe residues in myoglobin difficult without changing the direction of the residue to the heme group. We have overcome this problem by using the periodicity of α helices in cytochrome b_{562} to explore the dependence of energy flow in the protein on the heme–Trp distance.[82] Figure 4A shows the crystallographic structure of cytochrome b_{562} from *Escherichia coli*.[83] The advantage of cytochrome b_{562} over myoglobin is its four-helix bundle structural motif. Because helices are periodic, we were able to shift the residue along the helices in equidistant increments to measure the excess energy without altering its direction to the heme group. Furthermore, since WT cytochrome b_{562} has no Trp residue, it is simple to create mutants with a single Trp residue that serve as a probe of excess energy without causing structural instability in the protein.

Five cytochrome b_{562} mutants were generated by introducing a single Trp probe residue: R98W, L94W, A91W, L14W, and I17W. Heme is linked to the polypeptide chain through Met7

and His102. As illustrated in Figure 4B, the 98th, 94th, and 91st residues in the D helix are one, two, and three turns away from His102. Two and three turns separate the 14th and 17th residues from Met7 in the A helix. The periodic locations of these sites allowed us to examine the distance dependence of the vibrational energy transfer by comparing the results for the mutants.[80]

Figures 4C and 4D show the temporal evolutions in the relative intensity of the pump-induced intensity difference of the anti-Stokes W18 band with respect to the band intensity in the probe-without-pump spectrum of the cytochrome b_{562} mutants. The temporal changes of the anti-Stokes intensities were fitted to a double-exponential function convoluted with an instrumental response function and are shown as solid lines. The mutants differed in both the amplitude of the intensity change and the time when the intensity change reached a peak magnitude. R98W mutant displayed the greatest amplitude intensity changes, followed by L14W, L94W, I17W, and A91W mutants in descending order. R98W mutant displayed the shortest peak time of the intensity changes, followed by L14W, L94W, I17W, and A91W mutants in increasing order. Consequently, Trp residues with greater amplitudes of intensity changes exhibited longer peak times.

Systematic mapping of the distance dependence was accomplished using the periodicity of the helices in the four-helix bundle structure. Molecular dynamics simulations were then conducted to determine the heme–Trp side chain distances of the mutants, since no crystallographic data are available for these cytochrome b_{562} mutants. Figures 4E and 4F show the dependence of the amplitude and the peak time on the distance determined by the molecular dynamics simulations. As the distance between heme and Trp increased, the amplitude and peak time of the intensity changes in the anti-Stokes UVRR bands decreased and increased, respectively.

The spatial distribution of the excess energy released by the heme group was compared quantitatively to that estimated using the classical two-boundary thermal diffusion model,[80] which was described in Section IIIA. The anti-Stokes intensities at 2 and 8 ps calculated based on the thermal diffusion model are depicted in Figure 4G as broken lines, which well reproduced the observed anti-Stokes band intensities. When energy flow in a single direction along the helices is taken into account, the agreement of the anti-Stokes band intensities in terms of the heme–Trp distance and the delay time implies that the protein interior is well approximated as a continuum medium in the energy flow in a single direction, which is contrast to the case of myoglobin described in Section IIIA.

IV. ENERGY TRANSDUCTION MECHANISM: ATOMIC CONTACTS

A. Vibrational energy transfer through atomic contacts

We investigated the pathway of heme–polypeptide energy transfer by examining energy transfer to amino acid residues contacting the heme group in myoglobin mutants.[84] In each mutant, an amino acid residue at position 43, 68, or 89, which is close to the heme group, was replaced with a Trp residue, as shown in Figure 5A. The distance from heme to the Trp43, Trp68, or Trp89 residue in each mutant was 6–7 Å. In these myoglobin mutants, the intrinsic Trp residues (Trp7 and Trp14) were not replaced because their intensity changes of the time-resolved anti-Stokes UVRR bands were found to be negligibly weak as compared with those of Trp68,[84] and replacement of the residues significantly reduced the efficiency of protein expression. Figure 5B compares the temporal evolutions of the anti-Stokes W18 band intensities of Trp43, Trp 68, and Trp89 residues in the time-resolved difference spectra of each mutant. The vertical axis indicates a pump-induced increase in the intensity of the anti-Stokes W18 band relative to that of

the probe-without-pump spectrum. Temporal changes were comparable across all mutants: band intensity rose until 6–8 ps, and subsequently decreased to practically zero within 50 ps. These findings suggest that vibrational energy was transported from heme to the 43rd, 68th, and 89th locations at similar rates.

These data provided insights into the mechanism of energy flow in proteins. The heme group is linked to the polypeptide chain through a His residue (His93). Thus, the distances between heme and Trp43, Trp68, and Trp89 along the main chain of the protein are very different. The energy transfer rate for the three sites would be entirely different if the excess energy was transmitted to the Trp residue via the main chain, however such a difference was not seen. According to the X-ray crystallographic data of the mutants, the heme group has nonbonded contacts with Trp43, Trp68, and Trp89 (Figure 5A).[79, 85] The similar rates of heme–Trp energy transfer suggest that the energy is transferred not through the heme–His93 covalent linkage and the protein main chain but rather through atomic contacts between the heme group and the residues.

The three Trp residues at different positions showed distinctly different amplitudes of band intensity changes (Figure 5B): amplitude was largest for Trp68, followed in descending order by Trp43 and Trp89. These observed variations suggest that the energy flow out of each Trp residue occurs at a different rate. We found that the amplitudes of the anti-Stokes band intensity changes were inversely correlated with exposure to the solvent water: the larger the exposure, the smaller the amplitude. The X-ray crystallographic data showed that Trp68 and Trp43 were buried inside the protein, whereas Trp89 was close to the protein surface, facing the solvent.[79, 85] The extent of exposure to solvent water was quantitatively evaluated using the solvent-accessible surface area calculated with a 1.4 Å radius probe sphere. The area was calculated to be 2.9, 5.1, and 12.7 $Å^2$ for Trp43, Trp68, and Trp89, respectively, which is inversely correlated with the amplitude of

band intensity change (Figure 5B). This correlation was accounted for by assuming that the excess energy of the Trp residue is efficiently accepted by the solvent water, which is consistent with our earlier findings about the involvement of the heme propionate groups of myoglobin in vibrational energy relaxation.[64, 65] The two propionate groups in myoglobin protrude on the protein surface and contact the solvent water. Computational studies indicated that the propionate groups serve as an efficient channel for the heme–water energy transfer.[86, 87] Inspired by these computational studies, we investigated the vibrational energy relaxation of heme without propionate group(s) and showed that the rate of heme energy relaxation decreases upon removal of the propionate groups,[64, 65] supporting that solvent water is an efficient acceptor of vibrational energy.

B. Rigorous examination of the atomic contact pathway using a mutant lacking the heme–polypeptide covalent bond

The study using the Trp43, Trp68, and Trp89 of myoglobin mutants led to the hypothesis that atomic contacts are the dominant pathway for vibrational energy transfer in proteins: the primary pathway for energy transfer from the heme group to the protein moiety is not the covalent bond between heme–His93 and the protein main chain, but instead the heme–residue atomic contacts. Subsequently, we examined this hypothesis more rigorously. To directly examine the contribution of the linkage between the heme group and the polypeptide chain to the energy transfer pathway, we investigated the vibrational energy flow in a myoglobin mutant lacking the covalent bond.[88] In this myoglobin mutant, H93G(Im), His93 was replaced by Gly, abolishing the sole covalent bond between heme and the polypeptide chain and create a cavity in the heme-binding pocket. The resultant cavity can be occupied by exogenous ligands such as imidazole (Im). We introduced a Trp residue at position 68 of the protein to investigate the energy flow

from the heme group to the protein moiety. We then compared the data obtained for the V68W (Figure 6A) and V68W/H93G(Im) mutants (Figure 6B) to examine the effect of the covalent bond between heme and the polypeptide chain on energy flow.

Figure 6C depicts the temporal evolution of the anti-Stokes W18 band intensities in the time-resolved difference spectra of the V68W and V68W/H93G(Im) mutants. The ordinate represents the ratio of the pump-induced intensity change of the W18 band to the band intensity in the probe-without-pump spectrum. Following heme excitation, the intensity of the anti-Stokes band grew until 8 ps and subsequently decreased to near zero at 50 ps for both mutants. The temporal profiles of anti-Stokes intensity changes of the V68W and V68W/H93G(Im) mutants were identical within experimental uncertainty, indicating that the covalent bond between heme and the polypeptide chain plays a negligible role in energy flow from the heme group to Trp68 and that van der Waals contacts are the dominant pathway for energy migration from heme to the Trp residue. The covalent bond was also shown to play a negligible role in the vibrational energy relaxation of heme.[89]

Kitao and his coworkers collaborated with us and conducted molecular dynamics simulations to compare the three-dimensional structures of the V68W and V68W/H93G(Im) mutants because X-ray crystallographic data were not available for the V68W/H93G(Im) mutant.[88] The calculated structures indicated that the backbone structures and the heme–Trp distances are very similar between the two mutants. Therefore, the heme group in the V68W/H93G(Im) mutant likely forms van der Waals contacts with surrounding amino acid residues, which are similar to those in the V68W mutant. The breaking of the covalent linkage between His93 and the polypeptide chain had little effect on the rate of the energy migration,[88] indicating that the van der Waals contacts between heme and its surroundings are the dominant channel for the vibrational energy

migration. This situation of a heme group surrounded by a polypeptide chain is similar to that of a solute molecule surrounded by solvent molecules in a solution, where the excess energy in the solute molecules is exchanged dynamically through collisions with the first solvation shell, then exchanged dynamically through collisions of the first solvation shell with the second layer of solvation molecules, and so on.[90, 91]

V. MICROSCOPIC VIEW OF VIBRATIONAL ENERGY TRANSFER: COMPACTNESS OF PROTEIN STRUCTURES

In Section IV, we discussed that atomic contacts are dominant pathways for vibrational energy flow in proteins, likely due to the high packing density of protein structures. The packing density of the protein interior is high, much like that of a dense liquid.[92] For a given protein, the polypeptide chain is folded into a characteristic compact structure in aqueous solution. The packing density of the protein is nearly maximized as evidenced by the fact that proteins have an order of magnitude lower isothermal compressibilities than organic liquids.[93] There are many atomic contacts in the heme-binding pocket of myoglobin between the protein moiety and the heme–His93 group. The high packing density supports the view that not only covalent and hydrogen bonds but also non-bonded contacts play essential roles in energy flow in proteins.

It should also be pointed out that there are regions of both low density and highly compact regions in a protein structure. The packing density inside proteins has been quantitatively analyzed and appears to be inhomogeneous,[94, 95] giving rise to anisotropy of structural changes[96] and of energy flow.[71, 97] The significance of packing and non-bonded contacts in energy transfer discovered in our experiments with myoglobin mutants revealed further how variation in packing within a protein governs anisotropic energy flow. The contribution of through-bond and through-

space transport mechanisms to the energy flow in biomolecules has been explored in a variety of systems using various computational approaches.[98-103] We found that atomic contacts between the heme group and adjacent amino acid residues are the dominant channel for energy transfer from the heme group to the protein moiety. Our findings will stimulate theoretical research into the mechanism of vibrational energy transport in proteins. Reid et al., for example, highlighted an inventive use of time-resolved vibrational spectroscopy to discover the relationship between a change in conformational entropy and a change in protein functional state, and gave an expression quantifying the link.[104]

Elucidation of the mechanism for vibrational energy flow is absolutely fundamental for understanding proteins. The characteristics of vibrational energy flow in proteins reflect the compact nature of protein structure. The rates of the energy flow are associated with those of reactions in the active sites in proteins. Therefore, our understanding of vibrational energy flow will become increasingly relevant to our understanding of the structure and function of proteins.

VI. VIBRATIONAL DENSITY OF STATES: MOLECULAR THERMOMETER

Anti-Stokes intensity tells us the extent of vibrationally excited populations, as shown in Sections III and IV. There, we discuss the anti-Stokes intensities of particular modes, W16 and W18 modes. One may wonder if the extent of vibrational excitation in particular modes reflects the extent of excitation in the whole molecule or not. Strictly speaking, the temperature of a molecular system is defined only when the entire system is in thermodynamic equilibrium. However, the transiently excited molecules discussed here are not in thermodynamic equilibrium. It is nontrivial to answer to what extent we can talk of “temperature” after the vibrational

excitation of molecules. To address this question, we compare occupation probabilities in equilibrium and those in nonequilibrium.[97]

For a system in equilibrium, the occupation probability, $N(\nu_i)$, for a vibrational mode of frequency ν_i of a mode i where the $v = 1$ level is occupied, is described by the Boltzmann factor,

$$N(\nu_i) \propto \exp\left(-\frac{h\nu_i}{k_{\mathrm{B}}T}\right). \quad (1)$$

For a system in a nonequilibrium state, the occupation probability was calculated under an assumption, that is, after the energy transfer to the Trp side chain, the vibrational energy is rapidly redistributed over a large number of fundamental and isoenergetic combination states of the side chain, resulting in the condition that each state is assumed to have equal weight.

In nonequilibrium states, the probability of finding a molecule in the range of a total energy between E and $E + dE$ in the mode i where the $v = 1$ level is occupied is given by

$$N_E(\nu_i)dE = \frac{\rho_i(h\nu_i)\rho_{\mathrm{r}}(E-h\nu_i)}{\rho(E)}dE, \quad (2)$$

where $\rho(E)$ is the density of states of the molecule at an energy E.[105] $\rho_i(h\nu_i)$ and $\rho_{\mathrm{r}}(E - h\nu_i)$ are the density of states of the mode i and that of the rest of the modes, respectively. The occupation probability of the vibrational state of mode i is given by integration of the energy distribution, $N_E(\nu_i)$, weighted by $P(E)$, a probability of finding the molecules with a total energy E, over E:

$$N(\nu_i) = \int \frac{\rho_i(h\nu_i)\rho_{\mathrm{r}}(E - h\nu_i)}{\rho(E)} P(E)\mathrm{d}E \quad (3)$$

We calculated the occupation probability for 3-methyl indole, a model compound of the Trp side chain.[97] The frequencies of the fundamental modes of 3-methyl indole were obtained by density functional theoretical calculations at the B3LYP/6-311G(d,p) level. The densities of vibrational states below 6000 cm^{-1} were calculated based on the normal mode frequencies.

Figure 7A shows its total energy distributions for three cases. The blue line represents the total energy distribution in equilibrium at 300 K, which was derived by multiplying the density of states by the Boltzmann distribution at 300 K. The total energy distribution of the green line is similar to that of the blue line but is shifted to the higher energy side by 1000 cm^{-1}. The red line depicts the equilibrium total energy distribution at 387 K. We calculated the distribution at 387 K because a temperature rise to 387 K is caused by the introduction of 1000-cm^{-1} energy to 3-methyl indole at 300 K in equilibrium.

Figure 7B presents a semi-logarithmic plot of the occupancy probability as a function of the vibrational frequency. The green circles in Figure 7B show the occupation probabilities for the total energy distribution shown by the green line in Figure 7A. The blue and red lines show the occupation probabilities for the equilibrium states at 300 and 387 K, respectively, which are identical to the Boltzmann factor at a given temperature. Although the energy distribution of the green line in Figure 7A is in nonequilibrium, the occupation probability shown by the green circles below 1700 cm^{-1} is very close to that in the Boltzmann distribution at 387 K. This agreement means that the vibrationally excited Trp residue behaves as if it had a high temperature in a canonical ensemble, which is called the internal temperature of the excited molecule.[28, 106] The similarity of the occupation probabilities in the equilibrium and the nonequilibrium conditions depended on the number of fundamental modes or the density of states of molecules. For example, for acetic acid, a model compound of the Asp side chain, the occupation probability for the nonequilibrium states remarkably deviated from that in the Boltzmann distribution (Figure 7D) due to the density of states of the Asp side chain being insufficiently high. The results of the calculation for model compounds of the amino acids except Gly and Pro were presented elsewhere.[97] In a large polyatomic molecule at high excitation, the

partial energy distributions of a selected vibrational mode with small excitations per mode agree for microcanonical and canonical total distributions, provided that the average total energies are identical.[105]

In the resonance condition, temperature affects not only populations in vibrationally excited states but also Raman cross sections. The temperature dependence of the Raman cross sections can be calculated based on transform theory.[107-110] We obtained the temperature-dependent Raman cross sections for the W16 and W18 bands of 3-methyl indole using the theory and calculated the relative Raman intensities of the W16 and W18 bands as a function of temperature.[97] The calculated results well reproduced the temperature dependence of the observed Raman intensities. Accordingly, the anti-Stokes UVRR band intensities of Trp residues give the internal temperature and are shown to be an appropriate quantity to evaluate the amount of excess energy under nonequilibrium conditions in proteins.

We have been utilizing the anti-Stokes intensities of the Trp bands to study energy flow in proteins. When time-resolved anti-Stokes UVRR spectroscopy was applied to the observations of the intraprotein energy flow in our first study,[69] we chose the Trp bands as a probe of the excess energy because Trp is the most intense UVRR scatterer. Later, we found that the Trp bands provide incomparable information on local temperature with a spatial resolution of a single residue under nonequilibrium conditions because Trp has the largest side chain and thus the highest density of states among the amino acids composing proteins. Accordingly, the anti-Stokes spectra of Trp residues serve as an excellent spectroscopic thermometer to study the energy flow in proteins in terms of high sensitivity and straightforward interpretation. Indeed, we have shown that the temperatures calculated on the basis of the W16 and W18 bands of the Trp residue in cytochrome *c* in a time-resolved spectrum agreed with each other within experimental

uncertainty, implying the ability of UVRR spectroscopy to determine the transient temperature of Trp residues.[97]

VII. PROTEIN HEATER

Our studies showed that the high atomic density of protein structures results in high thermal conductance in the protein moiety. This suggests that the heat releasability of proteins is high, suggesting their excellent potential as molecular heaters. Having elucidated in some detail the energy transfer mechanism in hemeproteins, we are currently developing hemeprotein-based molecular heaters.

We examined the heat releasability of horse myoglobin to solvent water following photothermal conversion on heme. The spectra in Figure 8A show Raman bands due to the OH stretching modes of solvent water for the 100-μM horse myoglobin aqueous buffer solution. The Raman spectra were measured using 405 nm probe light with continuous excitation of heme using a 532 nm laser at six different powers. Band intensities were normalized using the intensity at 3425 cm^{-1} as an isosbestic point, reported previously.[111, 112] Band shapes in the myoglobin solutions changed upon changing the laser power while no spectral change was observed for the buffer solution without protein. Figure 8B shows difference spectra obtained by subtracting the spectrum obtained without irradiation with the excitation laser. Positive and negative bands appeared at 3548 and 3180 cm^{-1} on the higher- and lower-frequency sides, respectively. As the excitation laser power increased, the amplitudes of these bands increased. Similar spectral changes were observed by increasing the bulk temperature of the myoglobin solution. The OH stretching bands are known to change with the bulk temperature[111-113] due to changes in the hydrogen-bond networks between water molecules.[114] Therefore, we concluded that the spectral

changes observed for protein solutions probed using 405 nm light resulted from the temperature change of the sample solution, showing that myoglobin serves as a protein heater. The absolute values of intensity differences between the positive and negative bands showed a linear relationship with the temperature rise. Figure 8C shows a plot of the temperature rise against the excitation laser power. The photoinduced temperature rise was estimated to be 3.3 K at the maximum laser power used in this experiment (125 mW), which is sufficiently large to activate thermosensitive proteins such as transient receptor potential vanilloid 1, 2, and 4[115] in cells and to induce cellular responses. Extensive studies are ongoing to develop more efficient protein heaters.

Protein-based molecular heaters will be extremely useful for studies of thermal biology. Nanometer-size heaters were developed for photothermal therapy, in which cancer-cell death is triggered by light-induced hyperthermia. To date, many materials have been used in photothermal therapy, including gold nanoparticles,[116-121] graphene and graphene oxide,[122, 123] and conjugated polymers.[124, 125] These materials show highly efficient photothermal conversion, but they can be harmful to cells. By contrast, protein-based molecular heaters are less likely to adversely affect cells and are a promising tool for studying thermal responses in living cells. In addition, protein heaters can be localized in specific organelles in cells when the proteins are expressed with a signal sequence. The recent development of molecular temperature probes has enabled precise measurements of temperature in cells and revealed non-uniform temperature distributions due to spontaneous intracellular local heat generation. For example, organelle-specific heat generation was observed in the nuclear region[126, 127] and near mitochondria in steady-state cells.[126] Changes in intracellular temperature were also observed throughout the cell cycle,[126, 128] and cellular temperature changes were detected arising from mitochondrial heat

generation upon chemical stimulation.[126, 129] Most noteworthy, signal transduction utilizing heat has been proposed, since the temperature rise associated with cellular activity leads to another physiological response.[130, 131] The development of protein-based molecular heaters will bring new research methodology to molecular biology, and particularly thermal biology.

VIII. OUTLOOK

The studies described in this Perspective illustrate several advances in our understanding of vibrational energy flow in proteins, which can be utilized in developing protein heaters. Here, we discuss the outlook for studies on vibrational energy flow in proteins.

Technical developments in protein expression will enable more systematic and extensive studies on vibrational energy flow in proteins. The development of nonnatural amino acids which have large Raman scattering or infrared absorption cross-sections will provide more sensitive probes of excess vibrational energy. Nonnatural amino acids suitable as efficient photothermal converters are also desired. Site-specific isotope-labeled residues are ideal probes with residue-specific resolution since labeling spectrally discriminates the residue without changing its chemical properties. Currently, Trp residues except for the probe Trp are replaced with Phe or Tyr residues to prepare proteins containing a single Trp residue, but these replacements can considerably decrease the expression yield and the stability of the protein. Residue-specific observation is possible by site-specific isotope labeling without changing the amino acid sequence. Moreover, systematic, protein-wide mutational scanning will allow complete mapping of the vibrational energy flow in proteins. Mutagenesis studies of native protein scaffolds are often hampered by the complexity of the natural scaffold. Thus, the design of backbone structures is essential for systematic studies of vibrational energy transfer, such as using *de novo*

design,[132-141] allowing us to more rigorously address the distance and orientation dependence of vibrational energy flow in proteins. These technical developments will increase the feasibility and sensitivity of time-resolved vibrational observations of vibrational energy flow, and help improve techniques for time-resolved molecular thermography.

More rigorous comparisons of experimental observations with computational results will advance our understanding of vibrational energy flow in proteins. For peptides, such joint experimental/computational approaches have already allowed us to quantitatively account for the competition between backbone and contact transport in a peptide.[53] Such collaborations remain out of reach for proteins, although various computational approaches have been developed to study energy flow in numerous proteins in great detail.[81, 87, 102, 142-147] Time-resolved experiments on vibrational energy flow often require mutants in which some residues are replaced with natural or nonnatural amino acid residues. Although crystallographic data for such mutants are mostly unavailable, molecular dynamics simulations can provide structural data for interpreting experimental data on mutants.[82, 88] Meaningful comparisons between experimental and computational results will be possible when the number of probe sites can be increased in time-resolved experiments because the preparation of mutants will be easier in future due to the technical developments in protein expression discussed in the preceding paragraph.

The connection between vibrational energy flow and protein function has been discussed in many papers.[104, 144, 147-149] For example, an energy exchange network model was proposed to illustrate energy conductivities between residues. It was shown that rates of vibrational energy transfer in myoglobin across nonbonded contacts interacting via short-range potentials are correlated with those of conformational dynamics, suggesting a relation between vibrational energy transfer rates and entropy associated with the dynamics of interacting residues.[104] In

addition, mapping differences in the energy exchange network between two functional states can identify residues important in the structural transition between states, indicating that networks are involved in allosteric transitions.[147, 149] In this regard, it is crucial to reveal the vibrational energy transfer across the subunit interface in oligomeric allosteric proteins and correlate it with cooperativity.[148, 150, 151] Linkage of the energy flow to allostery has been discussed in the context that the linkage allows excess energy stemming from ligand binding to be directed elsewhere and drive structural or dynamical changes.[152] We discussed the importance of atomic contacts in vibrational energy transfer and the compact nature of protein structures in Section V. The absence of internal void spaces is also crucial for successive structural changes to propagate to spatially distinct sites:[153, 154] hence, proteins are functionally compact.[155] The mechanisms underlying protein functions based on energy flow will be understood when the connections between energy flow to allostery are clarified experimentally and theoretically.

The development of protein heaters is a unique application of vibrational energy flow. Rational design will allow us to design proteins with high energy releasability from the heater site. Bright future prospects for protein heaters are represented by two technologies: live cell imaging with fluorescent proteins[156-161] and the manipulation of neurons through optogenetics.[162-169] The creation of fluorescent proteins that efficiently emit light has made it possible to observe intracellular dynamics in real time, giving rise to new molecular biology techniques. The success of fluorescent proteins relies on the fact that they are introduced into cells at the gene level and are produced solely by molecules within the cell. This means that the introduction of the fluorescent proteins is less toxic to cells and the number of the protein molecules per cell does not decrease with cell division. Thus, artificial proteins that are produced solely using intracellular ingredients are extremely useful as research tools for living cells. Many fluorescent

proteins have been patented and commercialized as research tools in science and medicine and protein heaters generated solely from intracellular molecules have similar potential. In optogenetics, light-driven ion transport proteins introduced into nerve cells modify the ion concentration in the cells upon light irradiation, enabling artificial control of neural signals and manipulation of the organism. This approach utilizes technology for manipulating ion concentrations using light. Protein-based molecular heaters enable the manipulation of intracellular temperature using light. Given the development of optogenetics to date and its wide range of applications, the future of protein-based molecular heaters using light to manipulate local intracellular temperature is extremely promising.

IX. SUMMARY

Recent developments in the study of vibrational energy flow in proteins were reviewed, including future perspectives for methodologies and applications. Understanding vibrational energy flow in proteins has shed light on thermal diffusion on the nanoscale. New insights into vibrational energy flow have been provided through systematic studies utilizing the stable folds of proteins, contributing not only to our understanding of energy transfer in proteins but also to its transfer in condensed phases. Furthermore, these insights will allow wide-ranging applications for heat manipulation, including the development of protein-based molecular heaters. Vibrational energy transfer in proteins is becoming crucial in thermal biology.

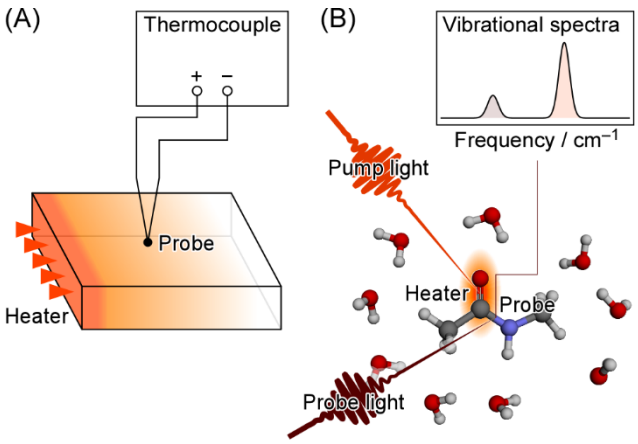

Figure 1. Schematic views of thermal diffusion. Macroscopic (A) and microscopic views (B).

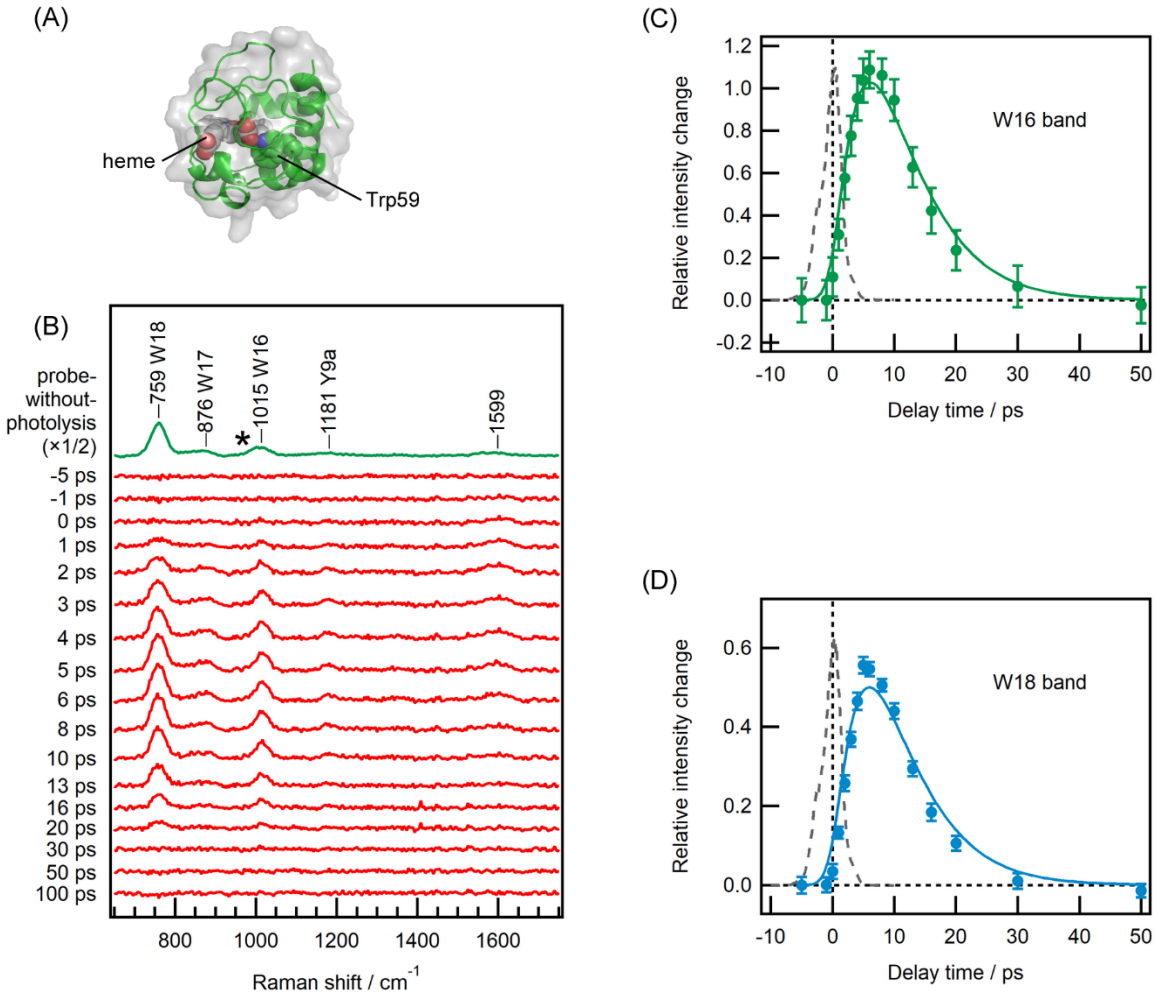

Figure 2. Vibrational energy flow in ferric cytochrome *c*. (A) Heme and the probe Trp residue in bovine ferric cytochrome *c* (PDB ID code 2B4Z). The protein is shown in green ribbon representation with a superimposed pale gray surface. Heme and Trp59 are shown as space-filling spheres. (B) Anti-Stokes UVRR spectra of ferric cytochrome *c* probed at 230 nm following heme photoexcitation at 405 nm. The top trace is the probe-without-pump spectrum, of which amplitude was multiplied by two. The sulfate band at 983 cm^{-1} marked by asterisk was used as a reference of Raman intensity. The remaining traces are time-resolved difference spectra obtained by subtracting the probe-without-pump spectrum from the pump-probe spectrum at each delay time. (C and D) Intensity changes in the anti-Stokes W16 (C) and W18 (D) bands from −5 to 50 ps. The circles represent the band intensity recorded at each delay time relative to the probe-without-pump spectrum. The solid lines were fit to a double-exponential function convoluted with the instrument response function, which is shown by broken lines. The best fit was obtained using the parameters 5.6_7±3.0 ps for the time constant of the rise and 5.6_8±3.0 ps for that of the decay of the W16 band. The rise and decay time constants for the W18 band were 5.5±2.5 and 5.6±2.5 ps, respectively. Figure panels modified with permission from N. Fujii, M. Mizuno, Y. Mizutani, J. Phys. Chem. B **115** (2011) 13057; copyright 2011 American Chemical Society; Y. Mizutani, Bull. Chem. Soc. Jpn. **90** (2017) 1344; copyright 2017 The Chemical Society of Japan.

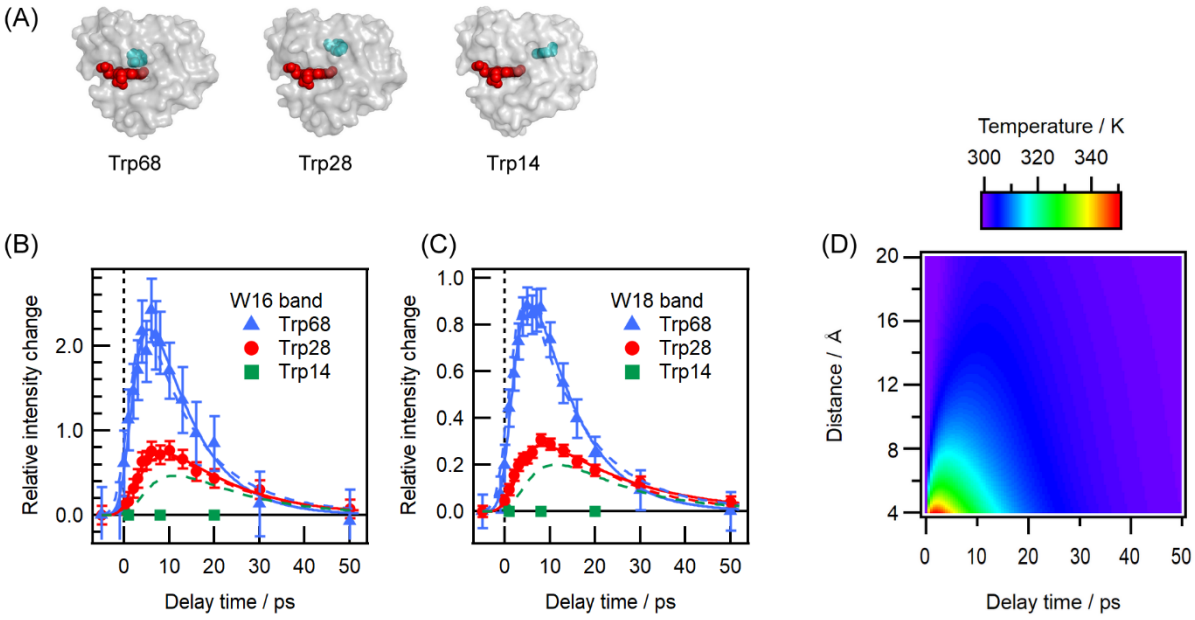

Figure 3. Vibrational energy flow in myoglobin mutants with the probe Trp residue at three different distances from heme. (A) Heme and the probe Trp residue in the mutants of sperm whale myoglobin. Red and blue space-filling spheres indicate heme and probe Trp residues, respectively. The protein is shown superimposed in pale gray surface representation. (B and C) Intensity changes in anti-Stokes W16 (B) and W18 bands (C) in the range from −5 to 50 ps upon heme excitation at 405 nm. The blue triangles, red circles, and green squares indicate the anti-Stokes band intensities of the Trp68, Trp28, and Trp14 mutants, respectively, recorded at each delay time relative to that in the probe-without-pump spectrum. The solid lines were fit to a double-exponential function convoluted with the instrument response function. The time constants obtained from the fit were as follows: W16 band of the Trp68 mutant, 3.0±0.7 ps for the rise and 9.2±1.8 ps for the decay; W16 band of the Trp28 mutant, 4.9±1.1 ps for the rise and 14.9±3.4 ps for the decay; W18 band of the Trp68 mutant, 3.0±0.4 ps for the rise and 9.6±1.0 ps for the decay; W18 band of the Trp28 mutant, 4.0±0.6 ps for the rise and 19.2±2.7 ps for the decay. The broken lines indicate temporal profiles of the intensities obtained from the Boltzmann factor calculated using the classical two-boundary thermal diffusion model. (D) Temperature as a function of heme–Trp distance and time calculated from the classical two-boundary thermal diffusion model for a solvated hemeprotein. Figure panels modified with permission from N. Fujii et al., J. Phys. Chem. Lett. **5** (2014) 3269, copyright 2014 American Chemical Society; Y. Mizutani, Bull. Chem. Soc. Jpn. **90** (2017) 1344; copyright 2017 The Chemical Society of Japan.

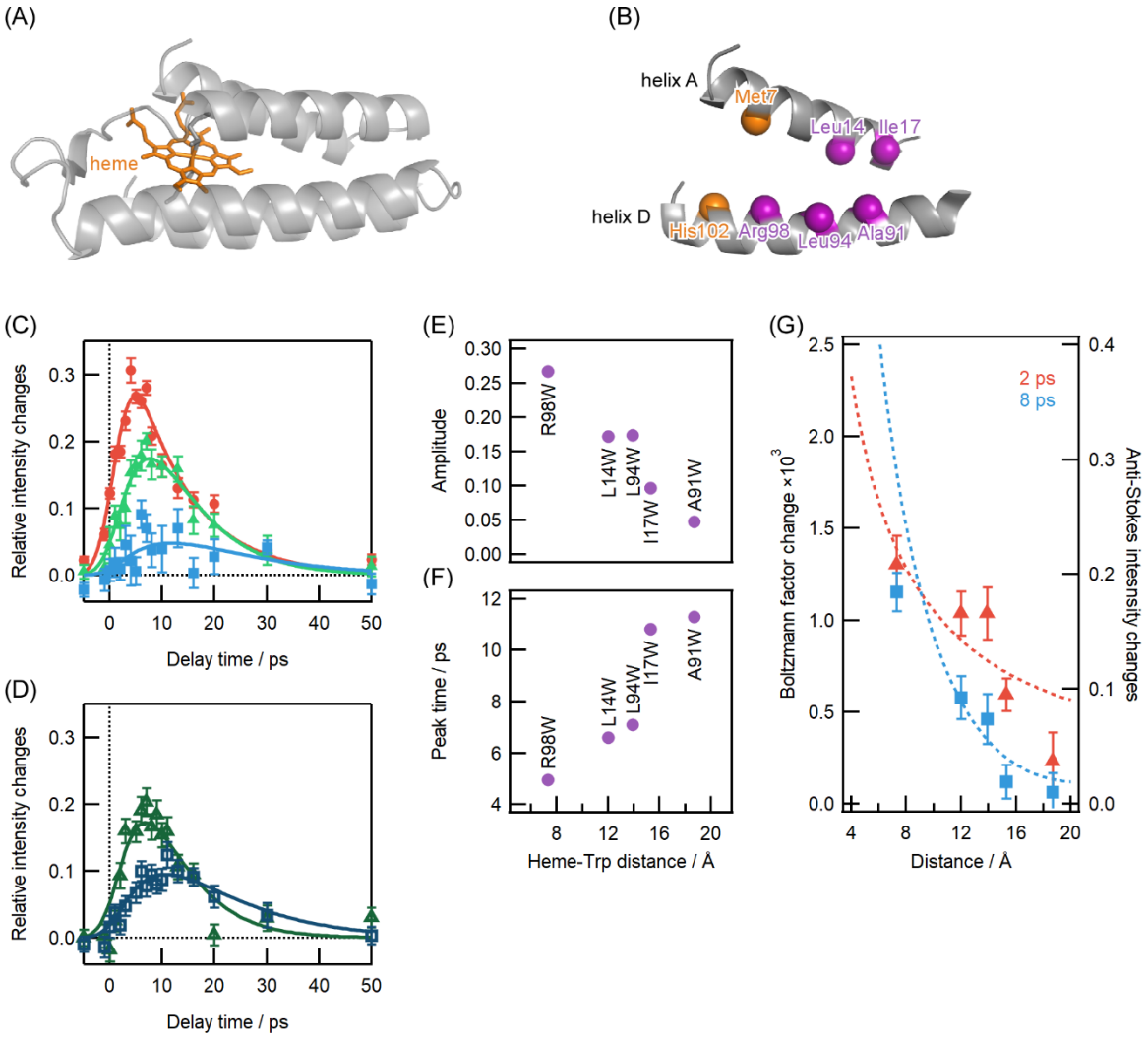

Figure 4. Vibrational energy flow in cytochrome b_{562} mutants with the probe Trp residue at five different distances from heme. (A and B) crystallographic structure of wild-type cytochrome b_{562} (PDB code: 256B). Panel A shows the overall structure. The heme group and coordinating residues (Met7 and His102) are shown in stick representation. Panel B illustrates positions of the probe Trp and the coordinating residues in the A and D helices of the mutants. Purple and orange spheres show the α carbons of Trp and the coordinating residues, respectively. (C and D) Intensity changes in the anti-Stokes W18 band in the range from −5 to 50 ps upon heme excitation at 405 nm; (C) mutations in helix D: Trp98, Trp94, and Trp91, and (D) mutations in helix A: Trp14 and Trp17. The solid lines were the best fits to a double-exponential function convoluted with the instrumental response function. The symbols in red, light green, light blue, dark green, and dark blue show the changes of intensity measured at each delay time relative to that in the probe-without-pump spectrum for the R98W, L94W, A91W, L14W, and I17W mutants, respectively. (E and F) Dependence of the amplitude (E) and peak time (E) of the pump-induced anti-Stokes W18 band intensity change on the heme–Trp indole-ring distance. The labels in the panels indicate the positions of the probe Trp residues. (G) Comparison of the observed anti-Stokes intensity changes with Boltzmann factor changes calculated based on the classical two-boundary thermal diffusion model. The blue squares and red triangles represent the observed anti-Stokes intensities at 2 and 8 ps, respectively. The changes in the Boltzmann factor are shown as broken lines. Figure panels modified with permission from S. Yamashita et al., J. Phys. Chem. B **126** (2022) 3283, copyright 2022 American Chemical Society.

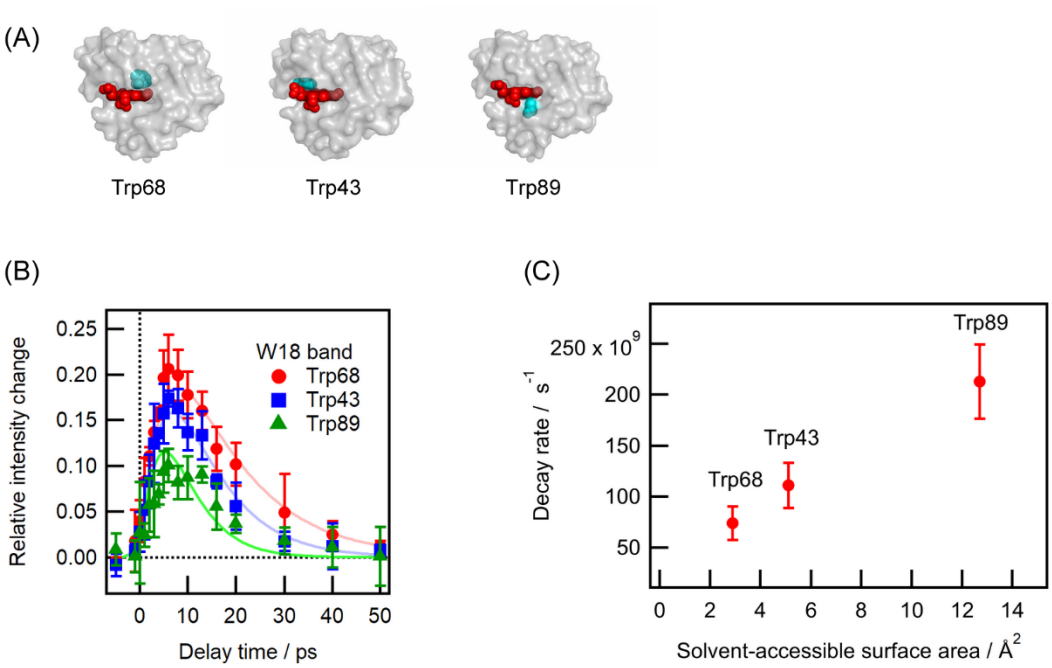

Figure 5. Vibrational energy flow in myoglobin mutants with the probe Trp residue close to heme. (A) Heme and the probe Trp residue in the mutants of sperm whale myoglobin. Red and blue space-filling spheres indicate heme and probe Trp residues, respectively. The protein is shown superimposed in pale gray surface representation. (B) Intensity changes in the anti-Stokes W18 band in the range from −5 to 50 ps upon heme excitation at 405 nm. The red circles, blue squares, and green triangles indicate the anti-Stokes band intensity of the Trp68, Trp43, and Trp89 mutants, respectively, recorded at each delay time relative to that in the probe-without-pump spectrum. The solid lines were fit to a double-exponential function convoluted using the instrument response function. (C) Decay rate of the pump-induced anti-Stokes W18 band intensity change of the Trp43, Trp68, and Trp89 residues plotted against the value of the solvent-accessible surface area at each Trp position. Figure panels modified with permission from M. Kondoh, M. Mizuno, Y. Mizutani, J. Phys. Chem. Lett. **7** (2016) 1950, copyright 2016 American Chemical Society; Y. Mizutani, Bull. Chem. Soc. Jpn. **90** (2017) 1344; copyright 2017 The Chemical Society of Japan.

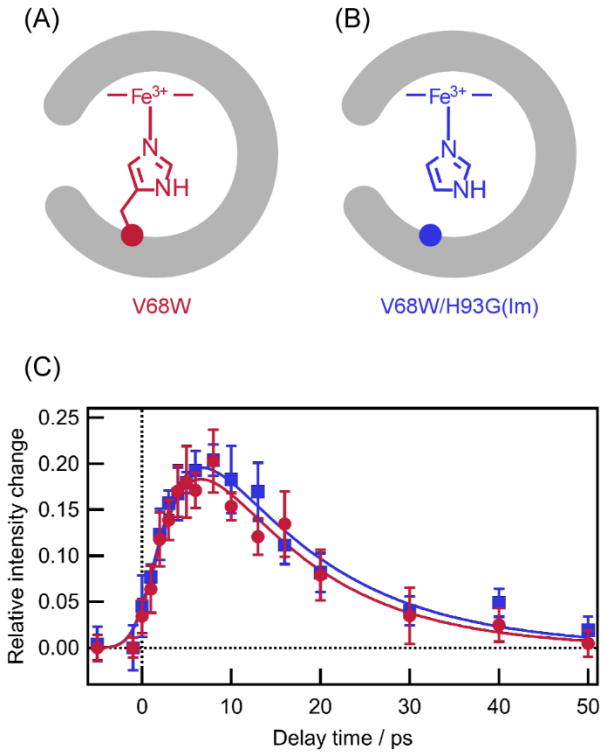

Figure 6. Vibrational energy flow in myoglobin mutants lacking the His93-polypeptide covalent bond. (A and B) Schematic views around the heme group in the myoglobin V68W (A) and V68W/H93G(Im) mutants (B). The proximal histidine is replaced by glycine in the V68W/H93G(Im) mutant (B). This substitution removes the only covalent linkage between the polypeptide chain and the heme group, resulting in a void that can be filled by exogenous ligands such as imidazole. In the V68W mutant (A), this covalent linkage is intact. (C) Intensity changes in the anti-Stokes W18 band in the range from −5 to 50 ps upon heme excitation at 405 nm. The red circles and blue squares indicate the anti-Stokes band intensity of the V68W and V68W/H93G(Im) mutants, respectively, recorded at each delay time relative to that in the probe-without-pump spectrum. The solid lines were fit to a double-exponential function convoluted using the instrument response function. Figure panels modified with permission from S. Yamashita et al., J. Phys. Chem. B **122** (2018) 5877, copyright 2018 American Chemical Society.

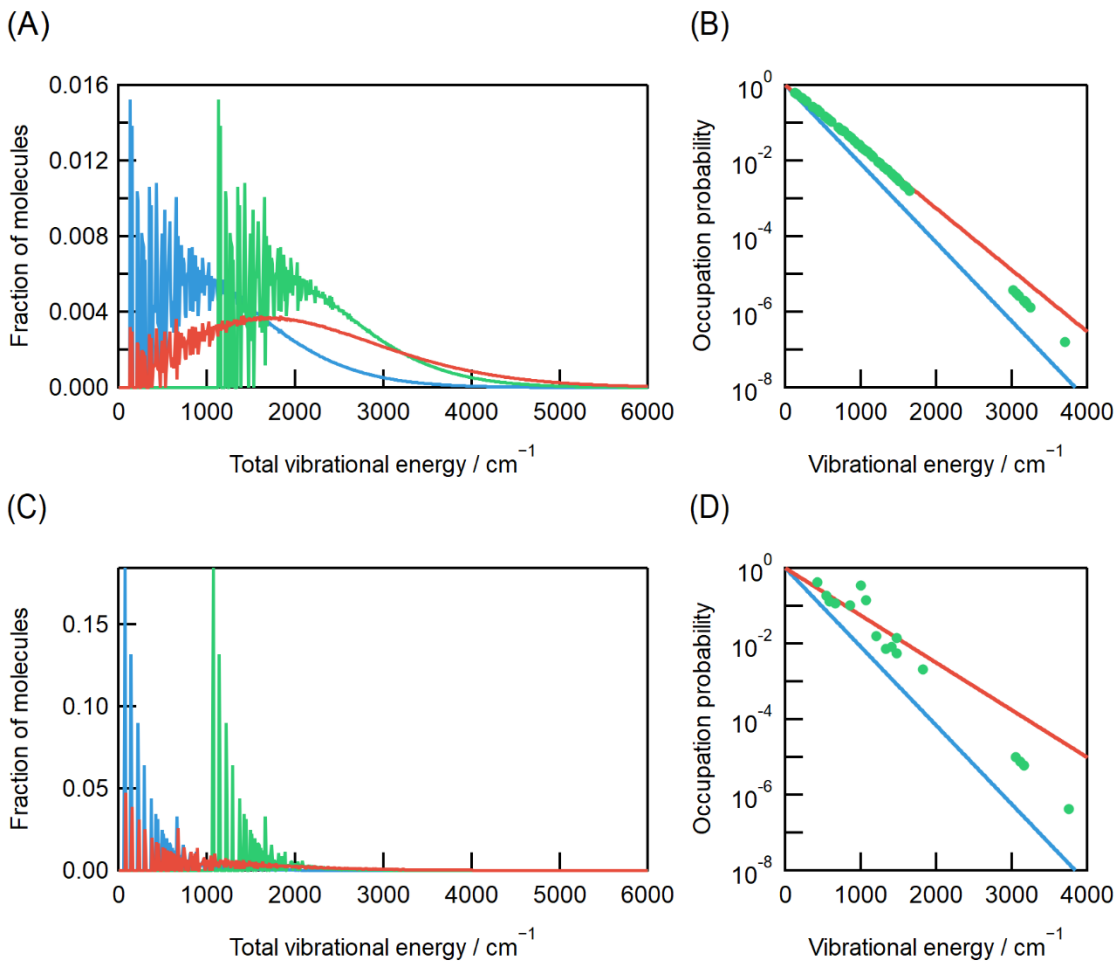

Figure 7. Vibrational energy distributions and occupation probabilities of 3-methyl indole and acetic acid as models of the Trp and Asp side chains. (A and C) The total energy distribution of 3-methyl indole (A) and acetic acid (B). In panel A, the blue and red lines show the total energy distribution in equilibrium at 300 and 387 K, respectively. In panel C, the blue and red lines show the total energy distribution in equilibrium at 300 and 499 K, respectively. In both panels, the green line shows the total energy distribution in nonequilibrium, where the distribution has the same form as the one shown by the blue line and is shifted to the higher energy side by 1000 cm^{-1}. (B and D) The occupation probability of 3-methyl indole (B) and acetic acid (D). In panel B, the blue and red lines show the total occupation probabilities at 300 and 387 K, respectively. In panel D, the blue and red lines show the total occupation probabilities at 300 and 499 K, respectively. In both panels, the green circles show the occupation probabilities for the total energy distribution shown by the green line in panels A and C. The fractions of molecules and the occupation probabilities are plotted on linear and log scales, respectively. Figure adapted with permission from S. Yamashita, M. Mizuno, and Y. Mizutani, J. Chem. Phys. **156** (2022) 075101, copyright 2022 American Institute of Physics.

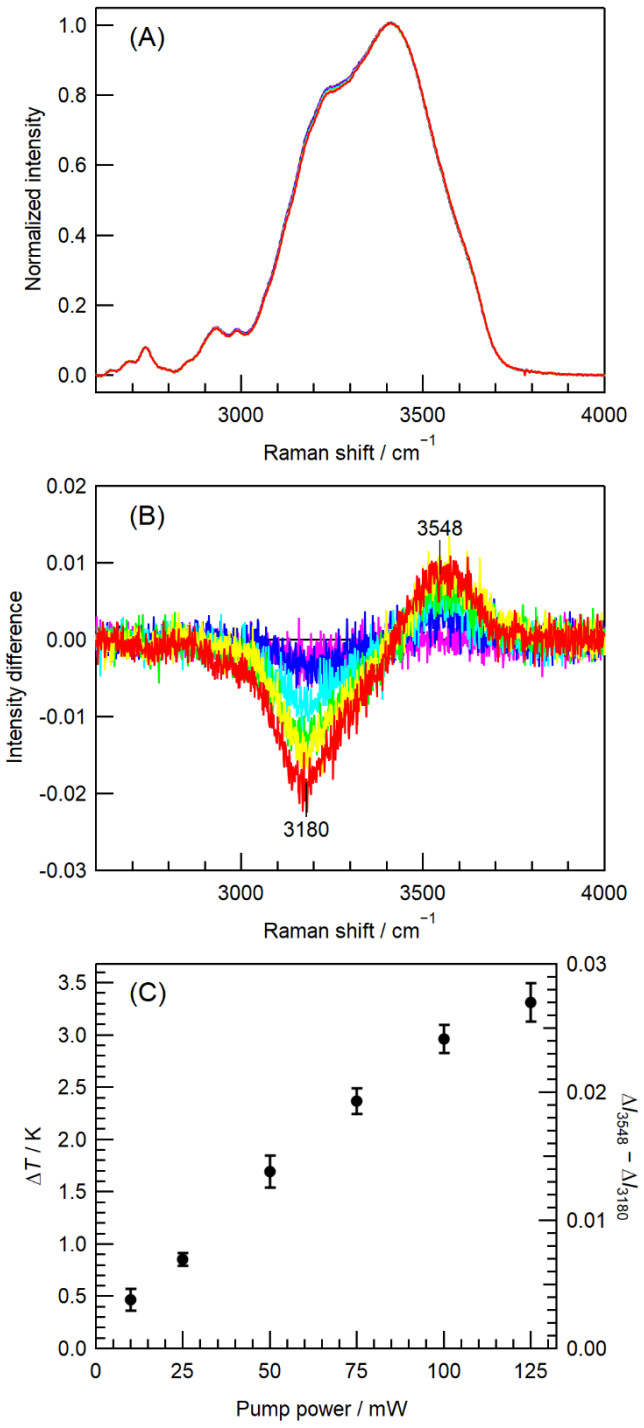

Figure 8. Photoinduced temperature rise of solvent water surrounding myoglobin. (A) Enlarged view of the Raman spectra of the OH stretching modes of solvent water in an aqueous solution of myoglobin. The probe wavelength was 405 nm. The red, yellow, green, cyan, blue, and purple traces are the spectra measured with continuous excitation using a 532 nm laser at a power of 125, 100, 75, 50, 25, and 10 mW, respectively. The black trace is the spectrum without irradiation of the excitation laser. The concentration of myoglobin was 100 μM and was dissolved in 50 mM HEPES buffer (pH 8.0). All measurements were carried out at 293.2 K,

controlled by a thermostat. Band intensities were normalized at 3425 cm^{-1}, reported as an isosbestic point for temperature dependence.[111, 112] (B) Difference spectra obtained by subtracting the spectrum without irradiation of the excitation laser. The trace colors correspond to those in panel A (excitation laser power levels). (C) Plots of the temperature rise against the excitation laser power. The photoinduced temperature rise was estimated based on the intensity differences between the positive 3548 cm^{-1} and negative 3180 cm^{-1} bands, which showed an approximate linear correlation with the bulk temperature on the right vertical axis.

Table I. Methods for the generation of vibrationally excited populations.

Photon-absorbing group	Type of transition	Wavenumber/cm^{-1}	Reference
(A) Direct excitation			
Carbonyl group in main chain	Vibrational transition, C=O stretching mode	1620–1750	44
Leucine-d_{10}	Vibrational transition, C–D stretching mode	2200	45
4-Azido-phenylalanine	Vibrational transition, antisymmetric N=N=N stretching mode	2114	50
(B) Indirect excitation via nonradiative transition			
Heme	Electronic transition	24700	69, 71, 82, 84, 88, 97
Copper porphyrin	Electronic transition	18200	46
Malachite green	Electronic transition	18200	46
Azobenzene[a]	Electronic transition	23500	44, 47-49
β-(1-Azulenyl)-alanine	Electronic transition	16300–16700	51-54
Gold nanoparticle	Electronic transition	19200	55

[a]covalently bound to peptides

Table II. Probes for vibrationally excited populations.

Probe group	Vibrational mode	Wavenumber/cm^{-1}	Reference
(A) Observation of hot bands in infrared spectra			
Carbonyl group in main chain	C=O stretching mode	1620–1750	44, 45, 47, 48, 55
4-Nitrophenylalanine	Symmetric NO_2 stretching mode	1346	49
Azidohomoalanine	Antisymmetric N=N=N stretching mode	2116	51-54
Azidoalanine	Antisymmetric N=N=N stretching mode	2113	54
4-Azido-phenylalanine	Antisymmetric N=N=N stretching mode	2027	54
4-Cyano-phenylalanine	C≡N stretching mode	2235	54
4-Cyano-tryptophan	C≡N stretching mode	2219	54
(B) Observation of anti-Stokes bands in resonance Raman spectra			
Trp side chain	W16 mode	760	69, 71, 82, 84, 88, 97
Trp side chain	W18 mode	1010	69, 71, 82, 84, 88, 97

ACKNOWLEDGMENT

We are grateful to Dr. Haruto Ishikawa, Dr. Masato Kondoh, Dr. Satoshi Yamashita, Mr. Naoki Fujii, Mr. Taro Watase, Prof. Akio Kitao, Dr. Duy Phuoc Tran, Dr. Hisham Dokainish, and Dr. Kazuhiro Takemura for their contributions to our work on energy flow in hemeproteins. This work was supported by the Ministry of Education, Culture, Sports, Science and Technology of Japan through a Grant-in-Aid for Transformative Research Areas (B) "Low-energy manipulation" to M.M. (JP20H05756), a Grant-in-Aid for Scientific Research on Innovative Areas "Soft Molecular Systems" to Y.M. (JP25104006), and by Grants-in-Aid for Scientific Research (B) to Y.M. (JP26288008 and JP20350007) from the Japan Society for the Promotion of Science.

AUTHOR DECLARATIONS

Conflict of Interest

The authors have no conflicts to disclose.

DATA AVAILABILITY

The data that support the findings of this study are available from the corresponding author upon reasonable request.

REFERENCES

[1] L. K. Iwaki *et al.*, Chem. Phys. Lett. **303** (1999) 176.
[2] J. C. Deàk, L. K. Iwaki, and D. D. Dlott, J. Phys. Chem. A **103** (1999) 971.
[3] G. Seifert *et al.*, J. Chem. Phys. **112** (2000) 6349.
[4] Z. Wang, A. Pakoulev, and D. D. Dlott, Science **296** (2002) 2201.
[5] N.-H. Seong, Y. Fang, and D. D. Dlott, J. Phys. Chem. A **113** (2009) 1445.
[6] Y. Fang *et al.*, J. Phys. Chem. A **113** (2009) 75.
[7] H. Bian, W. Zhao, and J. Zheng, J. Chem. Phys. **131** (2009) 124501.
[8] H. Bian *et al.*, J. Chem. Phys. **132** (2010) 184505.
[9] H. Bian *et al.*, J. Chem. Phys. **133** (2010) 034505.
[10] W. Zinth *et al.*, J. Chem. Phys. **78** (1983) 3916.
[11] H. Graener, and A. Laubereau, Chem. Phys. Lett. **102** (1983) 100.
[12] H. Graener, R. Dohlus, and A. Laubereau, Chem. Phys. Lett. **140** (1987) 306.
[13] E. J. Heilweil, R. R. Cavanagh, and J. C. Stephenson, J. Chem. Phys. **89** (1988) 230.
[14] H. Graener, Chem. Phys. Lett. **165** (1990) 110.
[15] H. Graener, G. Seifert, and A. Laubereau, Chem. Phys. Lett. **172** (1990) 435.
[16] H. J. Bakker, P. C. M. Planken, and A. Lagendijk, Nature **347** (1990) 745.
[17] H. J. Bakker *et al.*, J. Chem. Phys. **94** (1991) 1730.
[18] H. J. Bakker, P. C. M. Planken, and A. Lagendijk, J. Chem. Phys. **94** (1991) 6007.
[19] H. J. Bakker, J. Chem. Phys. **98** (1993) 8496.
[20] H. Graener, and G. Seifert, J. Chem. Phys. **98** (1993) 36.
[21] H. Graener, G. Seifert, and A. Laubereau, Chem. Phys. **175** (1993) 193.
[22] A. Tokmakoff, B. Sauter, and M. D. Fayer, J. Chem. Phys. **100** (1994) 9035.
[23] H. Graener, R. Zürl, and M. Hofmann, J. Phys. Chem. B **101** (1997) 1745.
[24] S. Woutersen, U. Emmerichs, and H. J. Bakker, J. Chem. Phys. **107** (1997) 1483.
[25] H.-K. Nienhuys *et al.*, J. Chem. Phys. **111** (1999) 1494.
[26] M. F. Kropman *et al.*, J. Phys. Chem. A **105** (2001) 4622.
[27] T. Elsaesser, and W. Kaiser, Annu. Rev. Phys. Chem. **42** (1991) 83.
[28] A. Seilmeier, and W. Kaiser, in *Ultrashort Laser Pulses*, edited by W. Kaiser (Springer, New York, 1993), p. 279.
[29] J. C. Owrutsky, D. Raftery, and R. M. Hochstrasser, Annu. Rev. Phys. Chem. **45** (1994) 519.
[30] J. C. Deàk *et al.*, Science **306** (2004) 473.
[31] Z. Wang *et al.*, Science **317** (2007) 787.
[32] Z. Wang *et al.*, Chem. Phys. **350** (2008) 31.
[33] J. A. Carter, Z. Wang, and D. D. Dlott, J. Phys. Chem. A **112** (2008) 3523.
[34] I. V. Rubtsov, and A. L. Burin, J. Chem. Phys. **150** (2019) 020901.
[35] D. Schwarzer *et al.*, J. Phys. Chem. A **106** (2002) 8019.
[36] Z. Lin, and I. V. Rubtsov, Proc. Natl. Acad. Sci. USA **109** (2012) 1413.
[37] L. N. Qasim *et al.*, J. Phys. Chem. C **120** (2016) 26663.
[38] N. I. Rubtsova, and I. V. Rubtsov, Chem. Phys. **422** (2013) 16.
[39] N. I. Rubtsova *et al.*, J. Phys. Chem. B **118** (2014) 8381.
[40] N. I. Rubtsova *et al.*, Acc. Chem. Res. **48** (2015) 2547.
[41] Y. Yue *et al.*, J. Phys. Chem. B **119** (2015) 6448.
[42] Z. Lin *et al.*, Phys. Chem. Chem. Phys. **14** (2012) 10445.

[43] D. M. Leitner, and J. E. Straub, *Proteins: Energy, Heat and Signal Flow* (CRC Press, Boca Raton, FL, 2009),
[44] E. H. G. Backus *et al.*, J. Phys. Chem. B **112** (2008) 9091.
[45] M. Schade *et al.*, J. Phys. Chem. B **113** (2009) 13393.
[46] G. Li, D. Magana, and R. B. Dyer, Nat. Commun. **5** (2014) 3100.
[47] V. Botan *et al.*, Proc. Natl. Acad. Sci. USA **104** (2007) 12749.
[48] E. H. G. Backus *et al.*, J. Phys. Chem. B **112** (2008) 15487.
[49] W. J. Schreier *et al.*, Peptide Sci. **100** (2013) 38.
[50] H. M. Müller-Werkmeister *et al.*, Angew. Chem. Int. Ed. **52** (2013) 6214.
[51] H. M. Müller-Werkmeister, and J. Bredenbeck, Phys. Chem. Chem. Phys. **16** (2014) 3261.
[52] T. Baumann *et al.*, Angew. Chem. Int. Ed. **58** (2019) 2899.
[53] E. Deniz *et al.*, Nat. Commun. **12** (2021) 3284.
[54] J. G. Löffler *et al.*, Angew. Chem. Int. Ed. **61** (2022) e202200648.
[55] M. Schade *et al.*, Nano Lett. **10** (2010) 3057.
[56] I. Harada, and H. Takeuchi, in *Advances in Spectroscopy: Spectroscopy of Biological Systems*, edited by R. J. H. Clark, and R. E. Hester (Wiley, New York, 1986), pp. 113.
[57] S. A. Asher, Annu. Rev. Phys. Chem. **39** (1988) 537.
[58] T. Kitagawa, Prog. Biophys. Mol. Biol. **58** (1992) 1.
[59] H. Takeuchi, Anal. Sci. **27** (2011) 1077.
[60] H. Takeuchi, Biopolymers **72** (2003) 305.
[61] P. M. Champion, and R. Lange, J. Chem. Phys. **73** (1980) 5947.
[62] J. W. Petrich, C. Poyart, and J. L. Martin, Biochemistry **27** (1988) 4049.
[63] Y. Mizutani, and T. Kitagawa, Science **278** (1997) 443.
[64] M. Koyama, S. Neya, and Y. Mizutani, Chem. Phys. Lett. **430** (2006) 404.
[65] Y. Gao *et al.*, Chem. Phys. Lett. **429** (2006) 239.
[66] L. Genberg *et al.*, J. Phys. Chem. **91** (1987) 5521.
[67] L. Genberg *et al.*, Chem. Phys. **131** (1989) 81.
[68] T. Lian *et al.*, J. Phys. Chem. **98** (1994) 11648.
[69] N. Fujii, M. Mizuno, and Y. Mizutani, J. Phys. Chem. B **115** (2011) 13057.
[70] N. Mirkin *et al.*, Proteins: Structure, Function, and Bioinformatics **70** (2008) 83.
[71] N. Fujii *et al.*, J. Phys. Chem. Lett. **5** (2014) 3269.
[72] Q. H. Gibson *et al.*, J. Biol. Chem. **261** (1986) 10228.
[73] B. A. Springer *et al.*, Chem. Rev. **94** (1994) 699.
[74] T. Suzuki, and K. Imai, Cell. Mol. Life Sci. **54** (1998) 979.
[75] G. S. Kachalova, A. N. Popov, and H. D. Bartunik, Science **284** (1999) 473.
[76] M. Brunori, D. Bourgeois, and B. Vallone, J. Struct. Biol. **147** (2004) 223.
[77] K. Shikama, Prog. Biophys. Mol. Biol. **91** (2006) 83.
[78] I. Sirangelo *et al.*, Eur. J. Biochem. **267** (2000) 3937.
[79] J. S. Olson, J. Soman, and G. N. Phillips Jr, IUBMB Life **59** (2007) 552.
[80] P. Li, and P. M. Champion, Biophys. J. **66** (1994) 430.
[81] D. M. Leitner, Annu. Rev. Phys. Chem. **59** (2008) 233.
[82] S. Yamashita *et al.*, J. Phys. Chem. B **126** (2022) 3283.
[83] F. Lederer *et al.*, J. Mol. Biol. **148** (1981) 427.
[84] M. Kondoh, M. Mizuno, and Y. Mizutani, J. Phys. Chem. Lett. **7** (2016) 1950.
[85] Y. Watanabe, H. Nakajima, and T. Ueno, Acc. Chem. Res. **40** (2007) 554.
[86] I. Okazaki, Y. Hara, and M. Nagaoka, Chem. Phys. Lett. **337** (2001) 151.

[87] D. E. Sagnella, and J. E. Straub, J. Phys. Chem. B **105** (2001) 7057.
[88] S. Yamashita *et al.*, J. Phys. Chem. B **122** (2018) 5877.
[89] X. Ye *et al.*, J. Phys. Chem. A **107** (2003) 8156.
[90] Y. Mizutani, and T. Kitagawa, J. Mol. Liq. **90** (2001) 233.
[91] K. Iwata, and H.-o. Hamaguchi, J. Phys. Chem. A **101** (1997) 632.
[92] J. Tsai *et al.*, J. Mol. Biol. **290** (1999) 253.
[93] K. Gekko, and Y. Hasegawa, Biochemistry **25** (1986) 6563.
[94] J. Liang, and K. A. Dill, Biophys. J. **81** (2001) 751.
[95] M. B. Enright, and D. M. Leitner, Phys. Rev. E **71** (2005) 011912.
[96] L. U. L. Brinkmann, and J. S. Hub, Proc. Natl. Acad. Sci. USA **113** (2016) 10565.
[97] S. Yamashita, M. Mizuno, and Y. Mizutani, J. Chem. Phys. **156** (2022) 075101.
[98] N. Ota, and D. A. Agard, J. Mol. Biol. **351** (2005) 345.
[99] P. H. Nguyen, P. Derreumaux, and G. Stock, J. Phys. Chem. B **113** (2009) 9340.
[100] L. Martínez *et al.*, J. Phys. Chem. Lett. **2** (2011) 2073.
[101] A. A. S. T. Ribeiro, and V. Ortiz, J. Phys. Chem. B **119** (2015) 1835.
[102] D. M. Leitner *et al.*, J. Chem. Phys. **142** (2015) 075101.
[103] S. Buchenberg, D. M. Leitner, and G. Stock, J. Phys. Chem. Lett. **7** (2016) 25.
[104] K. M. Reid, T. Yamato, and D. M. Leitner, J. Phys. Chem. B **122** (2018) 9331.
[105] H. Hippler, J. Troe, and H. J. Wendelken, J. Chem. Phys. **78** (1983) 5351.
[106] N. Gottfried, A. Seilmeier, and W. Kaiser, Chem. Phys. Lett. **111** (1984) 326.
[107] B. R. Stallard *et al.*, J. Chem. Phys. **80** (1984) 70.
[108] B. R. Stallard *et al.*, J. Chem. Phys. **78** (1983) 712.
[109] K. T. Schomacker, and P. M. Champion, J. Chem. Phys. **90** (1989) 5982.
[110] K. T. Schomacker, O. Bangcharoenpaurpong, and P. M. Champion, J. Chem. Phys. **80** (1984) 4701.
[111] G. E. Walrafen *et al.*, J. Chem. Phys. **85** (1986) 6970.
[112] G. E. Walrafen, M. S. Hokmabadi, and W. H. Yang, J. Chem. Phys. **85** (1986) 6964.
[113] T. Sugimura, S. Kajimoto, and T. Nakabayashi, Angew. Chem. Int. Ed. **59** (2020) 7755.
[114] Q. Sun, Vib. Spectrosc **51** (2009) 213.
[115] M. Tominaga, and M. J. Caterina, J. Neurobiol. **61** (2004) 3.
[116] X. Huang *et al.*, J. Am. Chem. Soc. **128** (2006) 2115.
[117] S. Lal, S. E. Clare, and N. J. Halas, Acc. Chem. Res. **41** (2008) 1842.
[118] E. C. Dreaden *et al.*, Chem. Soc. Rev. **41** (2012) 2740.
[119] N. S. Abadeer, and C. J. Murphy, J. Phys. Chem. C **120** (2016) 4691.
[120] A. Gharatape *et al.*, RSC Advances **6** (2016) 111482.
[121] M. R. K. Ali, Y. Wu, and M. A. El-Sayed, J. Phys. Chem. C **123** (2019) 15375.
[122] C. Chung *et al.*, Acc. Chem. Res. **46** (2013) 2211.
[123] V. Georgakilas *et al.*, Chem. Rev. **116** (2016) 5464.
[124] H. S. Jung *et al.*, Chem. Soc. Rev. **47** (2018) 2280.
[125] Y. Wang *et al.*, ACS Appl. Polym. Mater. **2** (2020) 4258.
[126] K. Okabe *et al.*, Nat. Commun. **3** (2012) 705.
[127] R. Piñol *et al.*, Nano Lett. **20** (2020) 6466.
[128] R. Yamanaka *et al.*, Biochem. Biophys. Res. Commun. **533** (2020) 70.
[129] N. Inomata *et al.*, Sens. Bio-Sens. Res. **27** (2020) 100309.
[130] Y. Hoshi *et al.*, J. Neurosci. **38** (2018) 5700.
[131] Y. Li *et al.*, Nat. Commun. **11** (2020) 4837.

[132] L. Regan, and W. F. DeGrado, Science **241** (1988) 976.
[133] P. B. Harbury *et al.*, Science **282** (1998) 1462.
[134] B. Kuhlman *et al.*, Science **302** (2003) 1364.
[135] L. A. Joachimiak *et al.*, J. Mol. Biol. **361** (2006) 195.
[136] N. Koga *et al.*, Nature **491** (2012) 222.
[137] A. R. Thomson *et al.*, Science **346** (2014) 485.
[138] S. E. Boyken *et al.*, Science **352** (2016) 680.
[139] P.-S. Huang, S. E. Boyken, and D. Baker, Nature **537** (2016) 320.
[140] P.-S. Huang *et al.*, Nat. Chem. Biol. **12** (2016) 29.
[141] Z. Chen *et al.*, Nature **565** (2019) 106.
[142] M. Takayanagi, H. Okumura, and M. Nagaoka, J. Phys. Chem. B **111** (2007) 864.
[143] D. M. Leitner, J. Chem. Phys. **130** (2009) 195101.
[144] R. Gnanasekaran, J. K. Agbo, and D. M. Leitner, J. Chem. Phys. **135** (2011) 065103.
[145] J. Helbing *et al.*, J. Phys. Chem. A **116** (2012) 2620.
[146] J. K. Agbo *et al.*, Theor. Chem. Acc. **133** (2014) 1504.
[147] T. Ishikura *et al.*, J. Comput. Chem. **36** (2015) 1709.
[148] D. M. Leitner, J. Phys. Chem. B **120** (2016) 4019.
[149] K. Ota, and T. Yamato, J. Phys. Chem. B **123** (2019) 768.
[150] K. M. Reid, T. Yamato, and D. M. Leitner, J. Phys. Chem. B **124** (2020) 1148.
[151] D. M. Leitner, C. Hyeon, and K. M. Reid, J. Chem. Phys. **152** (2020) 240901.
[152] A. A. S. T. Ribeiro, and V. Ortiz, Chem. Rev. **116** (2016) 6488.
[153] T. Shionoya *et al.*, J. Phys. Chem. B in press.
[154] S. Tahara, M. Mizuno, and Y. Mizutani, J. Phys. Chem. B **124** (2020) 5407.
[155] Y. Mizutani, Bull. Chem. Soc. Jpn. **90** (2017) 1344.
[156] D. C. Prasher *et al.*, Gene **111** (1992) 229.
[157] R. Heim, A. B. Cubitt, and R. Y. Tsien, Nature **373** (1995) 663.
[158] R. Y. Tsien, Annu. Rev. Biochem. **67** (1998) 509.
[159] R. H. Newman, M. D. Fosbrink, and J. Zhang, Chem. Rev. **111** (2011) 3614.
[160] J. R. Enterina, L. Wu, and R. E. Campbell, Curr. Opin. Chem. Biol. **27** (2015) 10.
[161] E. A. Rodriguez *et al.*, Trends Biochem. Sci. **42** (2017) 111.
[162] E. S. Boyden *et al.*, Nat. Neurosci. **8** (2005) 1263.
[163] T. Ishizuka *et al.*, Neurosci. Res. **54** (2006) 85.
[164] F. Zhang *et al.*, Nature **446** (2007) 633.
[165] B. Y. Chow *et al.*, Nature **463** (2010) 98.
[166] L. Fenno, O. Yizhar, and K. Deisseroth, Annu. Rev. Neurosci. **34** (2011) 389.
[167] K. Deisseroth, Nat. Neurosci. **18** (2015) 1213.
[168] E. G. Govorunova *et al.*, Science **349** (2015) 647.
[169] C. K. Kim, A. Adhikari, and K. Deisseroth, Nat. Rev. Neurosci. **18** (2017) 222.